Check for updates

Directly writing flexible temperature sensor with graphene nanoribbons for disposable healthcare devices†

Xue Gong,‡[ab] Long Zhang,‡[ab] Yinan Huang,‡[c] Shuguang Wang,[c] Gebo Pan [ID] *[ab] and Liqiang Li [ID] *[cd]

Disposable temperature sensors have great advantages in public health security and infectious disease control. However, complicated fabrication processes and poor performances persistently restrict their practical applications. In this paper, a flexible temperature sensor is firstly developed by directly writing or mask spraying commonly-used paper with a highly thermo-sensitive graphene nanoribbon (GNR) ink. The inexpensive, green materials and process endow the GNR sensors with the properties of being low cost, degradable and pollution free. The band gap and the local traps of GNRs, caused by the nanoscale effect and oxygen doping, make the sensor highly thermo-sensitive. The sensor also shows fast response, precise resolution and good bendable properties. As demonstrated, the sensor achieves monitoring of respiratory rate, measurement of body temperature, identification of human touch and constituting a 5 × 5 array for temperature mapping. These results demonstrate that the GNRs sensor is highly promising as an economical disposable device for personal healthcare and disease monitoring.

Introduction

Temperature sensors, serving as one of the key components of health monitoring devices, play an important role in personal healthcare and disease diagnosis.[1–4] The common devices for body temperature measurement, such as mercury thermometers and infrared thermometers, either conceal the potential risk of cross infection and mercury pollution or are limited by cost and inconvenience for continuous tracking.[5–10] Disposable wearable temperature sensors can be used for individual body temperature monitoring and significantly reduce the risk of cross infection,[11] especially in the hospital or quarantine where pathogens are highly concentrated. In order to develop a disposable wearable sensor for practical applications, both

highly sensing performances and low-cost manufacture must be taken into consideration. Unfortunately, most of the reported temperature sensors suffer from persistent limitations of poor performance (sensitivity,[3,12–14] response speed,[12,15–18] mechanical properties,[19–21] *etc.*) or cost issues (complicated fabrication process,[22–25] low efficiency,[3,26,27] pollution or biotoxicity,[16,28–31] *etc.*), which impedes their practical application for disposable healthcare devices. These issues may be solved through improving the properties and fabrication process of active materials.

Graphene, a single atomic 2D material, has sparked intense research interest in sensing applications due its good biocompatibility, excellent electric, optical and mechanical property.[32–36] Nevertheless, the highly conjugated structure and zero band gap[37,38] make it difficult to achieve a highly sensitive temperature response. Graphene nanoribbons (GNRs), as a quasi-one-dimensional derivative of graphene, has the suitable band gap that may yield great thermo-sensitivity.[39,40] More importantly, GNRs can obtain excellent solution processability,[41,42] which plays an essential role in the fabrication of low-cost disposable sensors. Furthermore, the relatively low defect density enables GNRs to maintain the good conductivity,[42,43] which renders the prepared sensors to directly operate without subsequent reduction process. These fascinating features make GNRs attractive in the application of disposable temperature sensors.

Here, we synthesized a high thermo-sensitive GNRs ink with excellent solution processability and further firstly prepared a disposable temperature sensor by directly writing or mask

[a]School of Nano-Tech and Nano-Bionics, University of Science and Technology of China, Hefei, Anhui 230026, People's Republic of China. E-mail: gbpan2008@ sinano.ac.cn

[b]Advanced Nano-materials Division, Suzhou Institute of Nano-Tech and Nano-Bionics (SINANO), Chinese Academy of Sciences, Suzhou 215123, Jiangsu, People's Republic of China

[c]Tianjin Key Laboratory of Molecular Optoelectronic Sciences, Department of Chemistry, Institute of Molecular Aggregation Science, Tianjin 300072, People's Republic of China. E-mail: lilq@tju.edu.cn

[d]Joint School of National University of Singapore, Tianjin University, International Campus of Tianjin University, Fuzhou 350207, Binhai New City, People's Republic of China

† Electronic supplementary information (ESI) available. See DOI: 10.1039/d0ra02815k

‡ These authors contributed equally to this work.

spraying on the commonly-used paper. Benefiting from the inexpensive, green materials and process, the paper-based GNRs sensor is low-cost, degradable and pollution free, which renders it great potential as a disposable device for health monitoring and diseases diagnosis. Interestingly, even though the novel concept sensor was roughly written on the paper, the high sensing performances and flexibility were obtained. Significantly, our sensor showed a high relative current change rate, $(I - I_0)/I_0 \times 100\%$ (referred as sensitivity here) of 172% with high cyclic stability, fast response time of 0.5 s, high temperature resolution of 0.2 °C. The sensor can maintain the almost constant sensitivity after up to 5000 cycles of bending at curvature radius of 1 cm due to the flexibility of GNRs and paper. As demonstrations, the sensor achieved monitoring of respiratory rate, measurement of body temperature, detection of the different temperature of water, identification of human touch and constituting a 5 × 5 array for temperature mapping.

Experimental

Materials

MWCNTs (diameter: 30–50 nm, length: <10 μm) and the MWCNTs conductive ink were purchased from Nanjing XFNANO Materials Tech. Co. Ltd and used without further purification. All the chemicals were purchased from Sinopharm Chemical Reagent Co. Ltd.

Synthesis of GNRs ink

Firstly, the MWCNTs were suspended in concentrated sulphuric acid (H_2SO_4, 98%) with magnetic stirring for 1 h under room temperature, and then the 500 wt% potassium permanganate ($KMnO_4$) was added slowly into the suspension. After stirring for 1 h, the reaction mixture was heated to 60 °C for 1 h and cooled to room temperature, then the mixture was slowly added into ice that contained 0.5 wt% hydrogen peroxide (H_2O_2).The resultant solution was centrifuged at 12 000 rpm for 10 minutes, finally the sediment was washed by hydrochloric acid solution (1 wt%) and deionized water for three times respectively to obtain purified GNRs. GNRs were dissolved in deionized water to form black ink (10 mg mL^{-1}). Glycerol (5 wt%) was added into the GNRs ink to enhance wettability to paper.

Fabrication of the paper-based GNRs sensors

The sensors were fabricated by writing and mask spraying the GNRs ink on the commonly-used paper. The Chinese word "Temperature" sensor was written by the Chinese brush stained with the GNRs ink. The bar thermometer-shaped temperature sensor was sprayed by a plastic mask (polyethylene glycol terephthalate (PET)). The 5 × 5 temperature sensor array was sprayed by a pair of metal mask. Firstly, the high conductive MWCNTs ink with almost no temperature response was sprayed by mask as electric circuits on the paper, and then the GNRs ink was sprayed by matched mask at the site between the two MWCNTs electrodes ($L \sim 50$ μm, $W \sim 1000$ μm). After drying at room temperature in air and encapsulated with scotch tape, the

GNRs sensor array was accomplished, without any further processing.

Characterization

SEM measurements were obtained from a Hitachi S-4800. TEM measurements were taken on a Tecnai G2 F20 S-TWIN. XRD measurements were tested on a Bruker AXS D8 Advance. Raman spectra were measured by a LABRAM HR with a 532 nm laser. XPS spectra were measured by an ESCALAB 250Xi. UV-vis spectra were obtained from a Lambda 750. Photographs were obtained from Huawei Mate 20. The electrical characterization of the temperature sensors was carried out by a Keithley 4200-SCS. The test bias voltage was set as 5 V. The variable temperature was obtained by a thermal platform that can quickly heat up and cool down.

Results and discussion

Device fabrication

The schematic diagrams of the fabrication process of GNRs sensors are shown in Fig. 1a. The GNRs were synthesized by longitudinally unzipping of economical multiwalled carbon nanotubes (MWCNTs), and could be well dispersed in deionized water to form black ink.[41,43] Firstly, the MWCNTs were suspended in concentrated sulphuric acid (H_2SO_4) with potassium permanganate ($KMnO_4$). The strong oxidizer and catalytic agent (H_2SO_4 and $KMnO_4$) split MWCNTs along the defects or crevasses, expanding them to obtain nanoribbons. The unzipping process introduced some oxygen-containing groups such as hydroxyl and carboxyl into the nanoribbons and generated doping. Fig. S1† shows the structure diagram of GNR. GNRs derived from this process has the following advantages: (1) remarkably, the hydroxyl and carboxyl endow GNRs the superior dispersity and stability in some polar solvents like water. Compared with another solution processible graphene derivative, Graphene Oxide,[44–47] GNRs can keep the suspension liquid with low viscosity and good liquidity rather than viscous gel even at high concentration (≥ 10 mg mL^{-1}); (2) the nanoscale lateral dimension and the oxygen groups may impart GNRs the certain band gap and local trap levels, and thus yield the high thermo-sensitivity, which would be discussed in more detail later; (3) the unzipping just causes mild damages to the conjunction of GNRs, and the good conductivity gets a retention in some degree, which means that the sensor written by GNRs can work without reduction processing. The excellent solution processability significantly simplifies the fabrication process of sensors, and the thermo-sensitive active material plays an indispensable role in high-precision temperature sensing, both of which are essential to achieve disposable sensors with low cost and high performance. Fig. S2† shows the photograph of the water-based GNRs ink with good dispersity.

In consideration of the low cost and flexibility required for disposable wearable sensors, the commonly-used paper was used as the substrate of GNRs sensor. The paper consists of fibers and is cheap, and the sensor thus is flexible and inexpensive, which implies that the paper-based GNRs sensor is
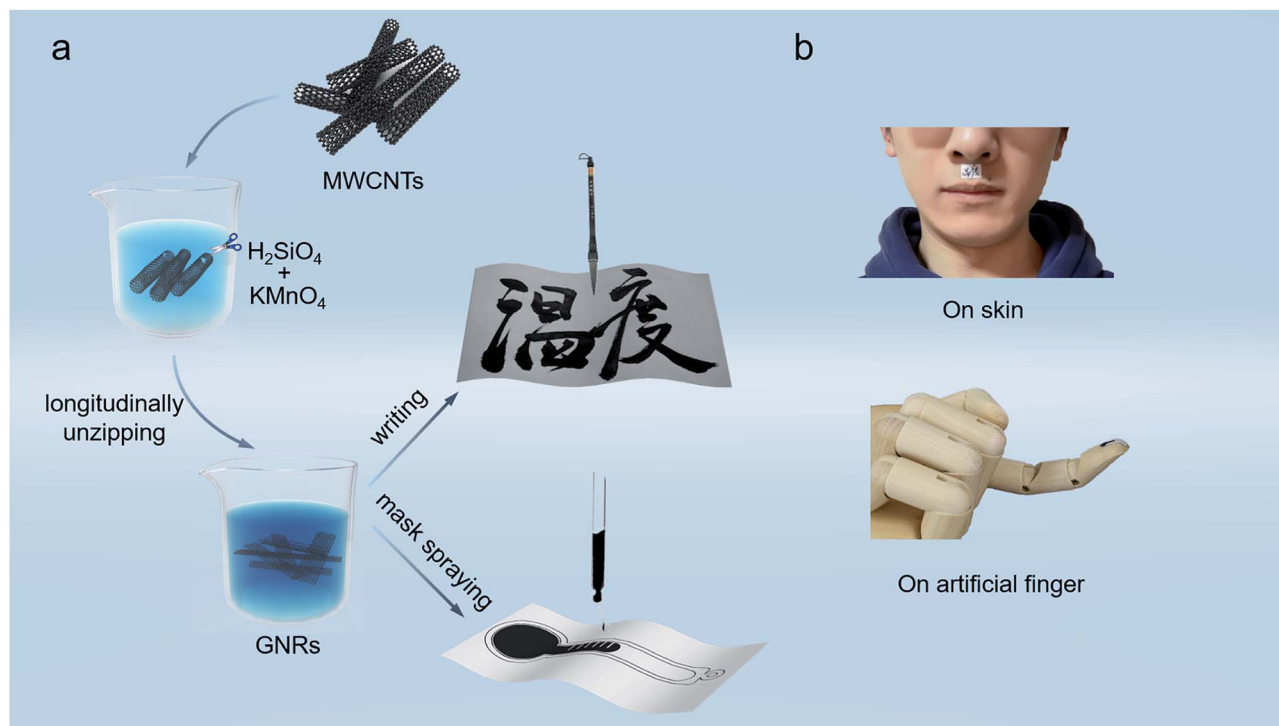
Fig. 1 (a) Schematic diagrams showing fabrication process of the paper-based GNRs sensors. (b) Demonstration photographs of the GNRs sensors adhering to human body and an artificial finger.

expected to become an economical disposable wearable device. To enhance wettability of the ink to paper, glycerol (5 wt%) was added into the GNRs ink, which significantly decreases the contact angle (about 90° to 30°) of ink on paper (Fig. S3†). It provides favorable conditions for the fabrication of the paper-based GNRs sensor. Specially, to demonstrate the easy fabrication of the sensor, the Chinese brush dipped in the GNRs ink was used to directly 'write' sensors on the paper. In this work, the Chinese word "Temperature" of cursive script was written as a conceptual temperature sensor. Except that, the sensor can also be prepared into any pattern by efficient mask spraying. As shown in Fig. 1a, a bar-thermometer-shaped temperature sensor was successfully sprayed on paper. The fabrication process of the paper-based sensor is one-step without any other post-processing, and thus is simple and high-effective. Deserve to be mentioned, the materials are innoxious and degradable, and can be recycled by commercial waste paper disposal project after use. It will effectively reduce the environmental pollution and waste of resources. The materials and fabrication technique endow the GNRs sensor potential to realize low cost and greenness: (1) the raw materials for fabricating GNRs sensors are mainly paper and GNRs, both of which are low cost, green, and recyclable. Paper, composed of cellulose fibers, is recyclable and environmentally friendly. GNRs mainly consist of carbon and oxygen and have been widely researched in biomaterial[48,49] and sewage treatment.[50–52] It demonstrates that GNRs have good biocompatibility and environmental friendliness. (2) The processing technology of GNRs sensors is simply printing without any post-processing, which can effectively save materials and

reduce the pollution. These advantages demonstrate the potential of the GNRs sensor as a new low cost and environmentally friendly device. Apart from the cost and greenness, benefiting by the flexibility of GNRs and paper, the GNRs sensor shows good flexibility and could be well attached on the skin or other curved surfaces. Fig. 1b exhibits the stable and conformal adhesion of the GNRs sensors on human skin and an artificial finger by thermal conductive silicone or scotch tape.

Analysis and characterization

To investigate the features of GNRs, multiple characterizations were performed. Fig. 2a and e show the scanning electron microscope (SEM) images of MWCNTs and GNRs, respectively. It can be clearly seen that there is a big difference between MWCNTs and GNRs. MWCNTs have large aspect ratio and relatively smooth edges, whereas the width of GNRs was enlarged obviously. The large-area SEM image of GNRs written on the surface of paper (Fig. S4†) demonstrates the uniform and continual active layer, which contributes to conductive property of sensor. The transmission electron microscope (TEM) images exhibit more details information. The multiple side walls of MWCNTs are clearly shown in Fig. 2b, and GNRs present a flat ribbon shape (Fig. 2f). These characterizations suggest the successful preparation of GNRs by longitudinally unzipping of pristine MWCNTs. In addition, the abundant oxygen-containing functional groups were introduced into GNRs during the unzipping process,[41,42] which was proven by both the appearance of the characteristic peak of oxide graphite (2θ at 12.4) in X-ray diffraction measurements (Fig. 2c and g) and the
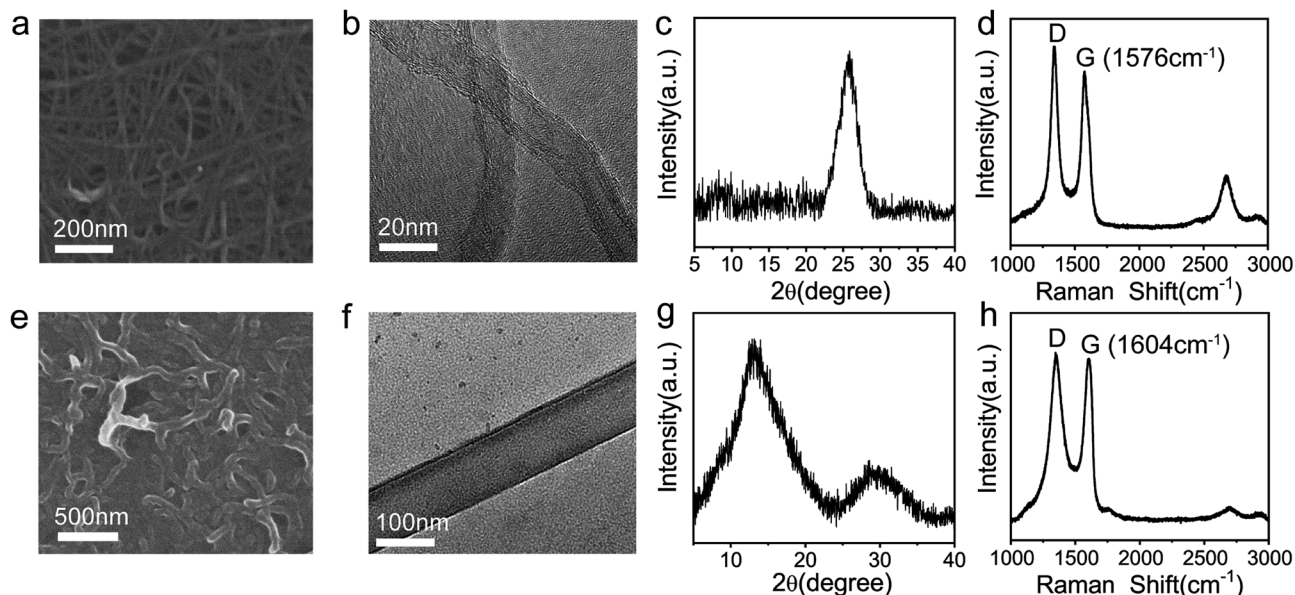
Fig. 2 SEM images of (a) MWCNTs and (e) GNRs. High resolution TEM images of (b) MWCNTs and (f) GNRs. X-ray diffraction patterns of (c) MWCNTs and (g) GNRs. Raman spectra of (d) MWCNTs and (h) GNRs.

upshifting of G band from 1576 cm^{-1} to 1604 cm^{-1} in Raman measurements (Fig. 2d and h) of MWCNTs and GNRs.[41,53,54] And the upshift near to 30 cm^{-1} of Raman wave number indicated that the introduction of oxygen generated the doping of GNRs.[55,56] X-ray photoelectron spectroscopy (XPS) demonstrates the definitive oxygen content and species of groups.

Fig. 3a shows the full XPS spectrum of MWCNTs and GNRs. The main XPS peaks at 284.8 and 533 eV correspond to the C 1s level and the O 1s level, respectively. The oxygen corresponding peak significantly enhanced in the spectrum of GNRs, definitely

revealing that many oxygens were introduced into GNRs during fabrication. The ratios of elements in MWCNTs and GRNs are shown in Table 1. The ratio of oxygen of MWCNTs is only 1.71% and that of GNRs is 29.9%. The peak-differentiation analysis of C 1s is shown in Fig. 3b, which reveals that the oxygen-containing groups in GNRs are hydroxyl (–C–OH at 287 eV) and carboxyl (–COOH at 288.8 eV).

These oxygen-containing functional groups introduce sp^3 hybridized orbital in GNRs, and damage the highly conjugated π–π structure of carbon atom, which causes some local traps in the energy band. Charge could be localized in these traps.[57,58] The localized carriers can be released into extend band and contribute to charge transport by thermal activation (Fig. 3d). Assuming that each of the local states traps one and only one carrier ($N_t = n_t$), the density of the released carriers can be expressed by following equation,

$$n_r = N_t \exp\left(-\frac{E_t}{k_B T}\right) \qquad (1)$$

where N_t is density of the traps, E_t is energy distribution of the local traps relative to the extend band, k_B is the Boltzmann's constant. The conductivity of GNRs can be given by the approximation formula $\sigma = e\mu n$, where σ is conductivity, e is

Fig. 3 XPS spectra of MWCNTs and GNRs: (a) full spectra, (b) fine spectra of carbon. (c) Plots of $(\alpha h\nu)^{1/2}$ against the photon energy in UV-vis absorption spectrum of GNRs. (d) Mechanism schematic diagram demonstrating thermal response of GNRs.

Table 1 Element information of C and O in XPS spectra of MWCNTs and GNRs

Sample	Element	Peak position (eV)	Atomic%
MWCNT	C 1s	284.8	98.29
	O 1s	531.93	1.71
GNR	C 1s	284.8	70.1
	O 1s	532.76	29.9

elementary charge and μ is mobility. The release of carriers will increase their density, elementary charge and μ is mobility. The release of carriers will increase their density, resulting the improvement of conductivity of GNRs. The release of the trapped carriers heavily depends on temperature, and thus plays an important role in achieving high temperature sensitivity of GNRs.

In addition, the oxygen doping and the nanoscale lateral dimension may lead to the certain band gap of GNRs. It is well known that graphene has zero band gap.[32,33,37] In the recent researches, doping[55,59,60] and nano-size effect have been reported as very effective ways to expand the band gap of graphene. The band gap of GNRs can be measured by UV-vis absorption spectrum (Fig. S5†). It had been reported that the gap nature of graphene gradually changes from direct to indirect with increasing accommodation of oxygen functional groups.[61] Therefore, the curve of $(\alpha h\nu)^{1/2}$ *versus* photon energy (Fig. 3c) was investigated. From approximate linear extrapolation, GNRs display apparent energy gap between 1.5 and 1.8 eV for indirect transition. For semi-metallic graphene, the increase of temperature only causes stronger lattice scattering, which decreases its conductivity. In contrast, the conductivity of GNRs with the suitable band gap improves with the increasing temperature due to the generation of free carriers through intrinsic excitation, which can be given by

$$n_i = \sqrt{N_c N_v} \exp\left(-\frac{E_g}{2k_B T}\right) \quad (2)$$

where n_i is intrinsic carrier concentration, N_c and N_v are density of conduction band and valance band, respectively, and E_g is band gap. Fig. 3d shows the schematic diagram of the above mechanism. On the one hand, some carriers trapped by the local levels in the forbidden band can be released to the extend band; on the other hand, the intrinsic excitation also contributes free carriers into extend band. It thus appears that the local levels and the band gap induced by oxygen-containing groups and the nanoscale lateral dimension are the reasons why the GNRs has high temperature sensitivity.

Electrical measurement

To investigate the sensing properties of the paper-based GNRs temperature sensor, the sensor was placed on a thermal platform that can quickly heat up and cool down. The temperature range was tuned between 30 °C to 80 °C with a step of 5 °C and the temperature rate was set as 1 °C s^{-1} and the interval time of temperature change was 20 s. A step-like curve with the variation of temperature is shown in Fig. 4a, which shows that the variation trend of the output signal of the sensor coincides well with the temperature setting curve. It directly demonstrates not only the capability of the sensor for real-time measurement but also the stability in a wide temperature range. Fig. 4b and c show the *I–V* curves and the plots of relative current change rate ($\Delta I/I_0 \times 100\%$, referred as sensitivity here) *versus* temperature, respectively. The sensitivity of GNRs sensor is as high as 172% in the temperature range of 30 °C to 80 °C, which is superior to most of the reliable wearable temperature sensors.[3,12–14,16,22,25,26,30,62] In

Fig. 4 (a) Step-like curve with the variation of temperature of the GNRs sensor. The right *y*-coordinate is corresponding temperature of normalized current change. (b) *I–V* curves of the sensor from 30–80 °C. (c) Plot of normalized current change *versus* temperature. (d) showing linear relationship between ln(*I*) and 1000/*T*.

addition, the sensitivity of the GNRs sensor can be defined by the temperature coefficient of resistance (TCR):

$$\text{TCR} = \frac{1}{R}\frac{dR}{dT} \times 100\% \quad (3)$$

where R is the base resistance at 293 K. The TCR of the GNRs sensor is from -1.89% to -0.82% K^{-1}, as shown in Fig. S6.† Furthermore, we also calculated the average value of TCR by:

$$\text{TCR}_{avg} = \frac{1}{R_{30}}\frac{R_{80}-R_{30}}{80-30} \times 100\% \quad (4)$$

The TCR$_{avg}$ of the GNRs sensor is 1.27% K^{-1}. The TCR for most metals is between 0.1–1% K^{-1},[63] and similarly, other conductive materials, such as single-walled carbon nanotubes (SWCNTs)[64] and poly(3,4-ethylenedioxythiophene)polystyrene sulfonate (PEDOT:PSS),[65] also exhibit a comparable sensitivity range. The TCR of Si nanowire is reported from -0.15 to -0.37% K^{-1}.[66] A linear relationship between ln(*I*) and 1000/*T* (Fig. 4d) shows a good fit with Arrhenius equation (linearity of 99.553%), which implies that the temperature response of GNRs comes from thermal activated electron and hole pairs. It completely accords with the above mechanism analysis. In addition, the output signal of the GNRs sensor well fits with a linear function, which may simplify the data post-processing of microchips and ensure the reliability of measurements in practical applications.

In the response speed test, an electric iron covered with PI tape was quickly in contact with and then removed away from the sensor. Fig. 5a shows the curve of the response and recovery. Remarkably, the sensor shows an impressive fast response time and a recovery time of about 0.5 s. In consideration of the time required by thermal conduction, the response speed of our sensor might be more remarkable. To the best of our
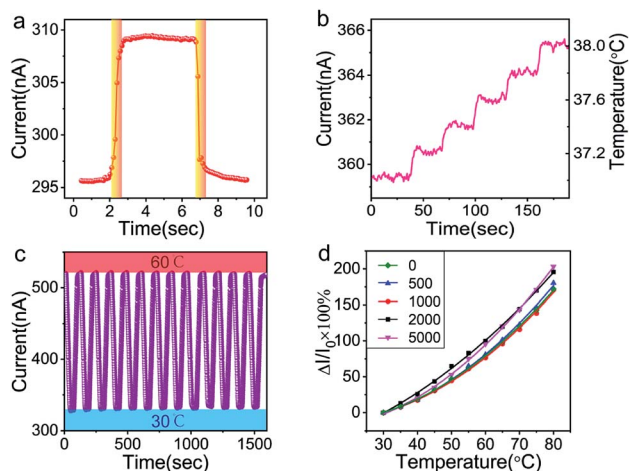
Fig. 5 (a) Response and recovery time of the GNRs sensor. (b) Step-like curve showing precise temperature resolution and high signal-to-noise ratio of the GNRs sensor. (c) Cyclic curves of the GNRs sensor in temperature range of 30–60 °C showing its operational stability. (d) Sensing performance of the GNRs sensor after manifold bending cycles at curvature radius of 1 cm.

knowledge, this value is much faster than most of the reported temperature sensors,[3,12,14–24,26,29,62] which indicates the advantages of its applications in real-time temperature monitoring. It is noted that the sensor could clearly distinguish the tiny temperature change as small as 0.2 °C over range 37 °C to 38 °C with high signal-to-noise ratio (Fig. 5b). The high resolution in the temperature range of human body can meet the requirements of monitoring body temperature. In fact, high sensitivity and signal-to-noise ratio suggest that our sensor may hold promise for higher resolution. However, due to the limitation of experimental setup, it is difficult to realize the smaller

temperature change in a continuous and reliable manner. Therefore, the test for higher resolution was not carried out for the sake of preciseness. The high resolution and the fast response of the paper-based GNRs sensor make it become a promising substitute of the slow-response mercurial thermometer in hospital. As a cheap one-off device, it can significantly reduce the risk of cross infection from different patients.

In addition, the cyclic sensing performance of the sensor was investigated over the temperature range of 30 °C to 60 °C (Fig. 5c), showing good stability in manifold cycles. Benefiting from the flexibility of GNRs and paper, the sensor exhibits an almost constant temperature response after up to 5000 cycles of bending at curvature radius of 1 cm (Fig. 5d). The high sensitivity, fast response speed, precise temperature solution, good repeatable stability and bendability demonstrate the wonderful advantages of the GNRs sensor in the applications of wearable sensors and health monitoring.

Application

Benefiting from high resolution and flexibility, the sensor can easily fit on the curved surface. The sensor was adhered above human lips by the scotch tape, and kept monitoring human respiratory rate in calm state through sensing temperature difference of breathing gas. As shown in Fig. 6a, the sensor unambiguously captured the human respiratory rate of about 13–14 times per minute in calm state, which profits from the fast response and high sensitivity. The capability of GNRs sensor to fast detect body temperature was also investigated. A GNRs sensor was attached to forehead, as shown in Fig. 6b, and the output signal changed distinctly and quickly when the sensor was stuck on and took down. Estimating with the plot of $\Delta I/I_0$ versus temperature in Fig. 4c, the corresponding temperature of electrical signal is about 35.8 °C, which approaches to
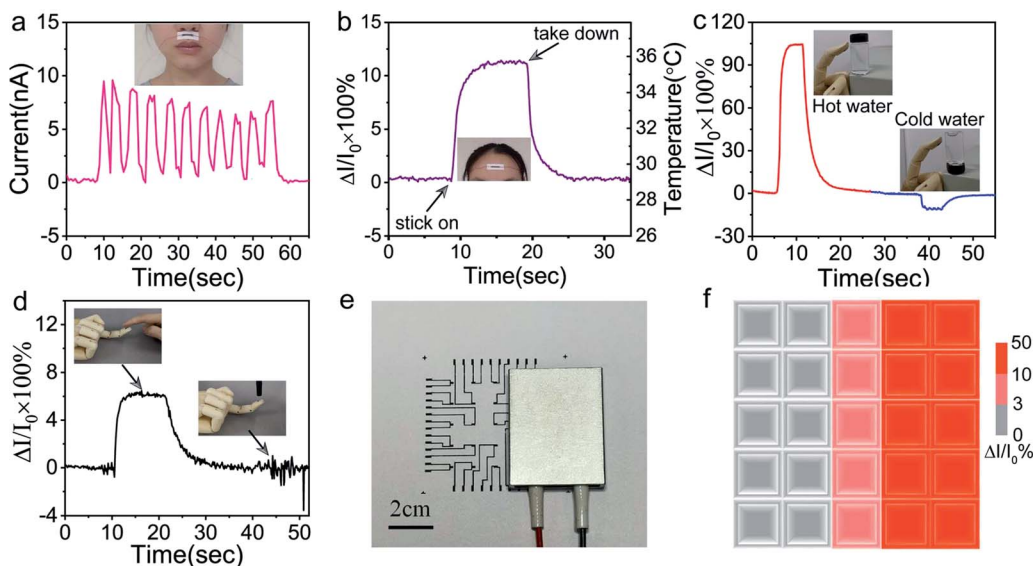

Fig. 6 (a) GNRs sensor was attached below the nose to monitor human respiratory rate in calm state through sensing temperature difference of breathing gas. (b) Measurement of human body temperature by the GNRs sensor adhered to the forehead. The GNRs sensor directly attached on the artificial hand for (c) sensing waters with different temperatures and (d) identifying human touch. (e) Photo of the GNRs sensor array covered a part by a hot plate. (f) Temperature distributions measured by the GNRs sensor array.

the 36 °C measured by infrared thermometer. We emphasized that the deviation was caused by misalignment of GNRs sensor and loose of data processing. As it turns out, GNRs sensor can fully satisfy the requirements for temperature detection in hospital and people's daily life as a one-off wearable device.

Furthermore, the potential application of the GNRs sensor for human–machine interaction was investigated. The sensor was pasted on the finger pulp of an artificial hand model by heat-conducting glue. When the finger touched the glass bottle, the sensor can clearly distinguish hot and cold water by the current changes, respectively (Fig. 6c). The sensor can endow artificial fingers the ability to recognize human touch. As shown in Fig. 6d, the human touch generated the legible temperature response signal, and the pressure exerted by the plastic pen caused only a weak signal disturbance, which shows high anti-interference ability to mechanical stimulation. In consequence, the sensor can identify the human touch from that of other things in the light of temperature contrasts.

Multipoint measurement is usually indispensable for practical applications. With this in mind, a 5×5 GNRs sensor array was fabricated for conducting temperature mapping. The high conductive MWCNTs with almost no temperature response was used as electric circuits on paper (see Experimental). The normalized current changes ($\Delta I/I_0 \times 100\%$) of the array were measured when a rectangular electric heater band was placed on it (Fig. 6e). Fig. 6f shows the mapping of the temperature distribution *via* the measurement of the normalized current changes. The mapping results depict the shape of heater successfully. This experiment exhibits precise temperature sensing capability of the GNRs sensor array and reveals its potential for the application in spatial temperature mapping.

Conclusions

In conclusion, aiming at developing high performance and economically disposable temperature sensors, we have demonstrated an efficiently-synthesized GNRs ink with high thermo-sensitivity and further prepared a flexible temperature sensor by directly writing or mask spraying with GNRs ink on commonly-used paper. The inexpensive materials and easy process make the GNRs sensor promising for an economical disposable health monitoring device. The nanoscale lateral dimension and oxygen doping of GNRs leads to the formation of the proper band gap and the local traps in the forbidden band, which enhances the thermal activated transporting and thus yields high thermo-sensitivity of the sensor. Remarkably, the sensor shows a high sensitivity of 172%, fast response time of 0.5 s, high temperature resolution of 0.2 °C and flexibility. We further demonstrated the applications of the GNRs in health monitoring and human–machine interaction, including monitoring of respiratory rate, measurement of body temperature, detection of the different temperature of water, identification of human touch and constituting a 5×5 array for temperature mapping. The development of the disposable GNRs sensors in this work holds great potential to bring more superior choices for health monitoring and disease diagnosing in public health security and infectious diseases control.

Conflicts of interest

The authors declare that they have no conflict of interest.

Acknowledgements

References

1 A. Chortos, J. Liu and Z. Bao, *Nat. Mater.*, 2016, **15**, 937–950.
2 S. T. Han, H. Peng, Q. Sun, S. Venkatesh, K. S. Chung, S. C. Lau, Y. Zhou and V. A. L. Roy, *Adv. Mater.*, 2017, **29**, 1700375.
3 S. Y. Hong, Y. H. Lee, H. Park, S. W. Jin, Y. R. Jeong, J. Yun, I. You, G. Zi and J. S. Ha, *Adv. Mater.*, 2016, **28**, 930–935.
4 T. Q. Trung and N. E. Lee, *Adv. Mater.*, 2016, **28**, 4338–4372.
5 M. Frobisher, L. Sommermeyer and M. J. Blackwell, *Appl. Microbiol.*, 1953, **1**, 187.
6 T. A. Baughman, *Environ. Health Perspect.*, 2006, **114**, 147–152.
7 F. A. Herrero, *JAMA, J. Am. Med. Assoc.*, 1973, **224**, 401.
8 D. Karunasagar, M. V. Balarama Krishna, Y. Anjaneyulu and J. Arunachalam, *Environ. Pollut.*, 2006, **143**, 153–158.
9 M. Bharara, J. E. Cobb and D. J. Claremont, *Int. J. Lower Extremity Wounds*, 2006, **5**, 250–260.
10 J. V. Craig, G. A. Lancaster, S. Taylor, P. R. Williamson and R. L. Smyth, *Lancet*, 2002, **360**, 603–609.
11 C. Dincer, R. Bruch, E. Costa-Rama, M. T. Fernandez-Abedul, A. Merkoci, A. Manz, G. A. Urban and F. Guder, *Adv. Mater.*, 2019, **31**, 1806739.
12 C. Y. Yan, J. X. Wang and P. S. Lee, *ACS Nano*, 2015, **9**, 2130–2137.
13 S. Harada, W. Honda, T. Arie, S. Akita and K. Takei, *ACS Nano*, 2014, **8**, 3921–3927.
14 P. Sun, M. Zhu, K. Wang, M. Zhong, J. Wei, D. Wu and H. Zhu, *ACS Appl. Mater. Interfaces*, 2013, **5**, 9563–9571.
15 C. Hou, H. Wang, Q. Zhang, Y. Li and M. Zhu, *Adv. Mater.*, 2014, **26**, 5018–5024.
16 N. T. Tien, S. Jeon, D. I. Kim, T. Q. Trung, M. Jang, B. U. Hwang, K. E. Byun, J. Bae, E. Lee, J. B. Tok, Z. Bao, N. E. Lee and J. J. Park, *Adv. Mater.*, 2014, **26**, 796–804.
17 T. Q. Trung, S. Ramasundaram, B. U. Hwang and N. E. Lee, *Adv. Mater.*, 2016, **28**, 502–509.
18 T. Q. Trung, N. T. Tien, D. Kim, J. H. Jung, O. J. Yoon and N. E. Lee, *Adv. Mater.*, 2012, **24**, 5254–5260.
19 A. Nakashima, Y. Sagawa and M. Kimura, *IEEE Sens. J.*, 2011, **11**, 995–998.
20 X. Ren, P. K. Chan, J. Lu, B. Huang and D. C. Leung, *Adv. Mater.*, 2013, **25**, 1291–1295.
21 J. Yang, D. Wei, L. Tang, X. Song, W. Luo, J. Chu, T. Gao, H. Shi and C. Du, *RSC Adv.*, 2015, **5**, 25609–25615.

22 Y. Hattori, L. Falgout, W. Lee, S. Y. Jung, E. Poon, J. W. Lee, I. Na, A. Geisler, D. Sadhwani, Y. Zhang, Y. Su, X. Wang, Z. Liu, J. Xia, H. Cheng, R. C. Webb, A. P. Bonifas, P. Won, J. W. Jeong, K. I. Jang, Y. M. Song, B. Nardone, M. Nodzenski, J. A. Fan, Y. Huang, D. P. West, A. S. Paller, M. Alam, W. H. Yeo and J. A. Rogers, *Adv. Healthcare Mater.*, 2014, **3**, 1597–1607.

23 J. Kim, M. Lee, H. J. Shim, R. Ghaffari, H. R. Cho, D. Son, Y. H. Jung, M. Soh, C. Choi, S. Jung, K. Chu, D. Jeon, S. T. Lee, J. H. Kim, S. H. Choi, T. Hyeon and D. H. Kim, *Nat. Commun.*, 2014, **5**, 574.

24 X. Ren, K. Pei, B. Peng, Z. Zhang, Z. Wang, X. Wang and P. K. Chan, *Adv. Mater.*, 2016, **28**, 4832–4838.

25 R. C. Webb, A. P. Bonifas, A. Behnaz, Y. Zhang, K. J. Yu, H. Cheng, M. Shi, Z. Bian, Z. Liu, Y. S. Kim, W. H. Yeo, J. S. Park, J. Song, Y. Li, Y. Huang, A. M. Gorbach and J. A. Rogers, *Nat. Mater.*, 2013, **12**, 938–944.

26 T. Q. Trung, S. Ramasundaram, S. W. Hong and N. E. Lee, *Adv. Funct. Mater.*, 2014, **24**, 3438–3445.

27 T. Yokota, Y. Inoue, Y. Terakawa, J. Reeder, M. Kaltenbrunner, T. Ware, K. Yang, K. Mabuchi, T. Murakawa, M. Sekino, W. Voit, T. Sekitani and T. Someya, *Proc. Natl. Acad. Sci. U. S. A.*, 2015, **112**, 14533–14538.

28 J. Jeon, H. B. Lee and Z. Bao, *Adv. Mater.*, 2013, **25**, 850–855.

29 X. Wu, Y. Ma, G. Zhang, Y. Chu, J. Du, Y. Zhang, Z. Li, Y. Duan, Z. Fan and J. Huang, *Adv. Funct. Mater.*, 2015, **25**, 2138–2146.

30 W. H. Yeo, Y. S. Kim, J. Lee, A. Ameen, L. Shi, M. Li, S. Wang, R. Ma, S. H. Jin, Z. Kang, Y. Huang and J. A. Rogers, *Adv. Mater.*, 2013, **25**, 2773–2778.

31 T. Xia, J. Wang, K. Jiang, Y. Cui, Y. Yang and G. Qian, *Chin. Chem. Lett.*, 2018, **29**, 861–864.

32 F. Bonaccorso, L. Colombo, G. Yu, M. Stoller, V. Tozzini, A. C. Ferrari, R. S. Ruoff and V. Pellegrini, *Science*, 2015, **347**, 1246501.

33 F. Bonaccorso, Z. Sun, T. Hasan and A. C. Ferrari, *Nat. Photonics*, 2010, **4**, 611–622.

34 Q. G. Zhu, J. Ma, X. C. Kang, X. F. Sun, J. Y. Hu, G. Y. Yang and B. X. Han, *Sci. China: Chem.*, 2016, **59**, 551–556.

35 Y. Zhang and W. Hu, *Sci. China, Ser. B: Chem.*, 2009, **52**, 751–754.

36 Y. Hou, T. Wu, L. Wang and P. Y. Feng, *Sci. China: Chem.*, 2013, **56**, 423–427.

37 X. Huang, X. Qi, F. Boey and H. Zhang, *Chem. Soc. Rev.*, 2012, **41**, 666–686.

38 R. Rong and S. Liu, *Chin. Chem. Lett.*, 2020, **31**, 565–569.

39 J. Cai, P. Ruffieux, R. Jaafar, M. Bieri, T. Braun, S. Blankenburg, M. Muoth, A. P. Seitsonen, M. Saleh, X. Feng, K. Mullen and R. Fasel, *Nature*, 2010, **466**, 470–473.

40 M. Y. Han, B. Ozyilmaz, Y. Zhang and P. Kim, *Phys. Rev. Lett.*, 2007, **98**, 206805.

41 D. V. Kosynkin, A. L. Higginbotham, A. Sinitskii, J. R. Lomeda, A. Dimiev, B. K. Price and J. M. Tour, *Nature*, 2009, **458**, 872–876.

42 L. Xiao, W. Xin, Z. Li, L. Sang and D. Hong, *Science*, 2008, **319**, 1229.

43 L. Jiao, L. Zhang, X. Wang, G. Diankov and H. Dai, *Nature*, 2009, **458**, 877–880.

44 D. Chen, H. Feng and J. Li, *Chem. Rev.*, 2012, **112**, 6027–6053.

45 S. Pei and H. M. Cheng, *Carbon*, 2012, **50**, 3210–3228.

46 Y. Huang, S. Wang, Z. Wang, X. Gong, Y. Meng, H. Li, Z. Tan, L. Yuan, J. Li, Y. Chen, L. Li and W. Hu, *Adv. Mater. Interfaces*, 2019, **6**, 1900365.

47 Z. Xu, K. Wu, S. Zhang, Y. Meng, H. Li and L. Li, *Mater. Horiz.*, 2017, **4**, 383–388.

48 B. Farshid, G. Lalwani, M. S. Mohammadi, J. S. Sankaran, S. Patel, S. Judex, J. Simonsen and B. Sitharaman, *J. Biomed. Mater. Res., Part A*, 2019, **107**, 1143–1153.

49 G. Lalwani, A. M. Henslee, B. Farshid, L. J. Lin, F. K. Kasper, Y. X. Qin, A. G. Mikos and B. Sitharaman, *Biomacromolecules*, 2013, **14**, 900–909.

50 L. Chen, R. Du, J. Zhang and T. Yi, *J. Mater. Chem. A*, 2015, **3**, 20547–20553.

51 L. R. Radovic, I. F. Silva, J. I. Ume, J. A. Menendez, C. A. Leon and A. W. Scaroni, *Carbon*, 1997, **35**, 1339–1348.

52 A. Dasgupta, J. Matos, H. Muramatsu, Y. Ono, V. Gonzalez, H. Liu, C. Rotella, K. Fujisawa, R. Cruz-Silva, Y. Hashimoto, M. Endo, K. Kaneko, L. R. Radovic and M. Terrones, *Carbon*, 2018, **139**, 833–844.

53 K. N. Kudin, B. Ozbas, H. C. Schniepp, R. K. Prud'homme, I. A. Aksay and R. Car, *Nano Lett.*, 2008, **8**, 36–41.

54 J. R. Rani, S. I. Oh and J. H. Jang, *Materials*, 2015, **8**, 8460–8466.

55 H. Liu, Y. Liu and D. Zhu, *J. Mater. Chem.*, 2011, **21**, 3335–3345.

56 S. Ryu, L. Liu, S. Berciaud, Y. J. Yu, H. Liu, P. Kim, G. W. Flynn and L. E. Brus, *Nano Lett.*, 2010, **10**, 4944–4951.

57 Y. D. Kim, M. H. Bae, J. T. Seo, Y. S. Kim, H. Kim, J. H. Lee, J. R. Ahn, S. W. Lee, S. H. Chun and Y. D. Park, *ACS Nano*, 2013, **7**, 5850–5857.

58 A. S. Sarkar and S. K. Pal, *J. Phys. D: Appl. Phys.*, 2015, **48**, 445501.

59 E. J. Duplock, M. Scheffler and P. J. Lindan, *Phys. Rev. Lett.*, 2004, **92**, 225502.

60 T. G. Pedersen, C. Flindt, J. Pedersen, N. A. Mortensen, A. P. Jauho and K. Pedersen, *Phys. Rev. Lett.*, 2008, **100**, 136804.

61 T. F. Yeh, F. F. Chan, C. T. Hsieh and H. Teng, *J. Phys. Chem. C*, 2011, **115**, 22587–22597.

62 C. Y. Lee, A. Su, Y. C. Liu, P. C. Chan and C. H. Lin, *Sensors*, 2010, **10**, 3363–3372.

63 D. C. Giancoli, *Physics: Principles with Applications*, Prentice Hall, 4th edn, 1995.

64 S. Y. Hong, Y. H. Lee, H. Park, S. W. Jin, Y. R. Jeong, J. Yun, I. You, G. Zi and J. S. Ha, *Adv. Mater.*, 2016, **28**, 930–935.

65 I. W. Kwon, H. J. Son, W. Y. Kim, Y. S. Lee and H. C. Lee, *Synth. Met.*, 2009, **159**, 1174–1177.

66 C. P. Wang, C. W. Liu and C. Gau, *IEEE Int. Conf. Nano/Micro Eng. Mol. Syst.*, 2011, **630**, 20–23.